

LOW-SUBSONIC AERODYNAMIC ANALYSES OF A NONPLANAR BWB MODEL: AN EXPERIMENTAL AND CFD STUDY

Melike Nikbay¹, Konstantinos Kontis², Hassan Aleisa² & Berkay Pirlepeli¹

¹Istanbul Technical University, Istanbul, 34469, Turkiye ²University of Glasgow, Glasgow, G12 8QQ, UK

Abstract

A nonplanar wing concept significantly improves the aerodynamic performance of an aircraft. Hence, adopting nonplanar flow control concepts is essential to achieve an enhanced lift performance and controllability. Likewise, the blended wing body (BWB) concept uses a combined wing and fuselage to create a single lifting surface throughout the entire wingspan. The BWB concept offers various advantages such as reduced operating cost, reduced noise emission, and improved aerodynamic efficiency. It was expected that a combination of both nonplanar and BWB model would exhibit better aerodynamic performance. This study investigated the aerodynamic performance of a combined nonplanar and BWB concept model using experimental and computational methods at various angles of attack. The experimental tests were conducted at the de Havilland low-speed wind tunnel facility at the University of Glasgow, while the numerical simulations were carried out using OpenFOAM 8.0. Additionally, optimization of the nonplanar wingtip shape was performed to improve the aerodynamic performance further. The aerodynamic characteristics and flowfield analyses of the wing model were presented and explained using the post-processed figures.

Keywords: Nonplanar, BWB; wind tunnel test; CFD

1. Introduction

The BWB configuration is an airfoil-shaped centerbody that combines propulsion, control surfaces, and payload. The BWB configuration is, in essence, a flying wing that must operate steadily across its entire flight envelope, carrying a payload with low structural weight drawback and producing lift with low drag drawback [1]. A significant amount of the total lift is produced by the centerbody, which lowers the wing loading. The low wing loading also guarantees good low-speed flight characteristics, negating the need for bulky high-lift systems like double-slotted flaps [2]. Investing in nonplanar flow control concepts is essential to achieve tailless flying BWB configurations with high lift performance and improved controllability. Nonplanar wing configurations are classified according to their aerodynamic properties or configuration features, and they are categorized, such as nonlinear aerodynamic concepts, closed lifting systems, multiple-wing designs, and tip devices [3]. Devices to disperse and interact with the vorticity in the vicinity of the wingtip region, taking advantage of the spiraling airflow in this region to create additional traction and reduce the induced drag have been investigated, such as winglets [4, 5, 6, 7], tip sails [8, 9, 10, 11], vortex diffusers [12], and multi-winglets [13, 14, 15]. A valuable review of the possibility of overall air vehicle efficiency enhancement by employing nonplanar wing concepts was provided [16, 17].

For wings of the same span and lift, the nonplanar wings provide a significantly better reduction in drag than planar wings [3]. However, implemented surface extensions to primary wings to get nonplanar wing geometry such as wing-winglets, C-wings, or box wings increase profile drag and higher bending moments due to increased wetted area and weight, respectively. Hence, the integration and assessment of nonplanar wing concepts represents a challenge, and the evaluation of nonplanar configurations must not only be done for a vortex drag decrease viewpoint. Furthermore, the design

factors should be considered, such as reducing the structural weight to enhance the aircraft's overall performance and the potential to increase high-lift and good stability and control features.

Whitcomb [4] used high aspect ratio winglets instead of low aspect ratio endplates to generate a significant variation in the vortex drag without a high increase in the wetted area. Heyson et al. [5] reported that winglets were preferable over span extensions by comparing two concepts with limited root bending moment. Verstraeten and Slingerland [18] studied the drag characteristics of optimally span-loaded planar, Winglet, and C-wings. They concluded that the wing with a winglet has an aerodynamic performance advantage over the C-wing and offers a drag decrease compared to a planar wing for wings with span and aspect ratio restrictions. Computational and experimental investigations of the behavior of different devices include Winglet, C-wing, fence, and gurney flap coupled with a swept back flying BWB model [19, 20]. They found that the c-wing displayed a reduced drag coefficient, whereas the Winglet demonstrated higher aerodynamic efficiency [19]. The growth of the use of winglets is justified by an increase in the wing's aerodynamic efficiency. Studies in this field have demonstrated the effectiveness of winglets.

An in-depth understanding of flow separation and its effects is required to improve the aerodynamic performance, such as stability and high-lift of the swept back flying BWB configurations. Generally, there are various types of flow separation, such as mixed, leading, and trailing edge separation. The type of flow separation depends on the wing geometry design and Reynolds number [21]. The swept back BWB models experience wingtip stalls during take-off and landing, which is detrimental to their stability and control. The stall inception occurs at the outboard wing section and then expands to the inboard wing section. This flow behavior causes the lift center to move forward, leading to the pitch-up of the swept back flying BWB configurations. The wingtip separation can be delayed by modifying the wing design or applying flow control devices. One such approach is implementing winglets to suppress the wingtip separation, improving the lift-to-drag ratio (C_L/C_D) with no more structural loads, resulting in better fuel efficiency, a more extended range, and a bigger payload. In the present study, the aerodynamic characteristics of a combined nonplanar and BWB concept model were assessed by employing experimental and numerical simulation approaches at different angles of attack (AOA). Additionally, optimization of the wingtip geometry was carried out to improve the aerodynamic characteristics further. The aerodynamic characteristics and vortex formation were analyzed using simulation results, including post-processed figures.

2. Nonplanar Tip-Section Optimized Model

A numerical optimum design approach is used to develop a nonplanar wingtip extension to enhance the aerodynamic efficiency of the swept back flying BWB model in [22, 23, 24]. The baseline wing model consists of three sections: the fuselage, the mid-section, and the tip-section. The nonplanar wingtip section of the model has been aerodynamically optimized to improve lift and control power, as well as the longitudinal stability margin. This modification can improve wing loading, structural stiffness, and shielding of the aileron outboard tip. Both high-fidelity and low-fidelity numerical aerodynamic solvers are used to evaluate aerodynamic performance. A surrogate-based optimization study is performed to improve the aerodynamic characteristics of the model. The developed surrogate models reflect the objective functions, and the design space is explored using uniform sampling. A derivative-free generic method is used to tackle the constrained optimization problem. Flow conditions are given in Table 1.

Table 1 – Flow conditions

Mach	0.0874	
Altitude	0	[m]
Dynamic Pressure	1488.68	$\left[\frac{kg}{ms^2}\right]$
Reynolds Number	1.5E06	- 1113

In the present optimization problem, the design variables, such as tip blending strength, tip sweep, and dihedral angle, are optimized to maximize the C_L/C_D . Incremental Latin hypercube sampling

(ILHS) is used to obtain the design points in the design space. Table 2 shows the bounds of the design variables.

Parameter	Initial	bound
Tip Sweep Angle	40	[30,60]
Tip Dihedral Angle	0	[-30,30]
Tip Blending Strength	1	[0.5,1.5]

Incremental Latin hypercube sampling is used during optimization to explore the design space more thoroughly. LHS incremental sampling preserves segmentation and correlation structure while generating new set samples. For a more accurate approximation model, the number of samples steadily increases during model creation. A total of 50 samples were created using the Latin Hypercube sampling method. A Kriging surrogate model is generated using 45 samples, and the model is cross-validated with the remaining 10% of the total samples. The formulation of the constrained optimization problem is as follows:

$$\min_{s \in S} \quad -\frac{C_L(s)}{C_D(s)}$$
 subject to
$$h_1(s) = \frac{b}{b_{ref}} - 1 = 0,$$

$$h_2(s) = \frac{l_f}{l_{fref}} - 1 = 0$$
 (1)

The swept back flying BWB model aerodynamic characteristics are analyzed using OpenFOAM 8.0 solver [32] within a flow domain developed identically to the wind tunnel test section. The inbuilt OpenFOAM grid generators, blockMesh + snappyHexMesh, discretize the flow domain. The k- ω SST model was chosen for the turbulence closure.

Surrogate models estimate the relation between the objective function and design variables in a given design space. The low-fidelity surrogate models can be used as an alternative to high-fidelity CFD simulations to reduce the total computational power required for the optimization process. The reduction in computational power increases with the number of design variables used for optimization. The workflow of the surrogate model generation is provided in Figure 1. Initially, the sampling of design space is done, and the data is obtained from the design points using the vortex lattice method (VLM). The vortex lattice method is computationally less expensive than the CFD simulations, making it more suitable for optimization processes that require lots of runs. The data received from the sample set is grouped into training and test data. The training data is used to create a model that optimizes the hyperparameters. Later, cross-validation is performed to access the models performance. It uses a set of data that was not analyzed early, and if the error magnitude is less than the given criteria, it validates the model. Conversely, if the error magnitude is higher than the given criteria, a new sample set with more design points is generated during the refinement step. The iterative process was repeated until the required convergence was achieved.

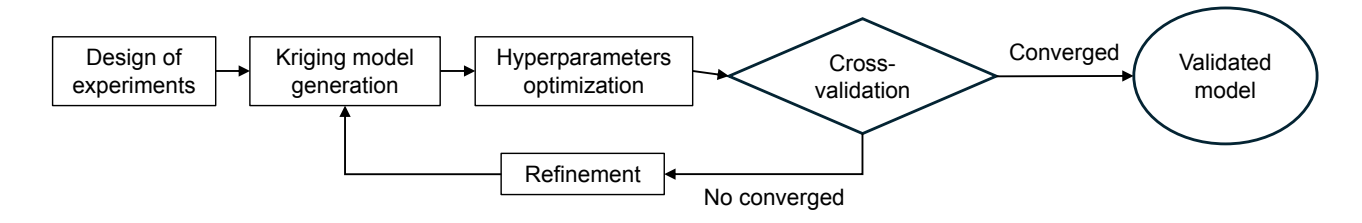


Figure 1 – Surrogate model generation process

The geometry was parameterized using three design variables, and a constrained optimization problem was solved using a genetic algorithm. The wingtip that was acquired is an extension of the wing

classified as a winglet, which enhances the aerodynamic efficiency of the wing by 11%. The wing tip extension that has been optimized effectively mitigates the pressure gradient at the wing tip in comparison to the planar wing configuration.

Table 3 – Best parameters

Parameter	Initial	Interval	Best
Tip Sweep Angle	40	[30,60]	56.4
Tip Dihedral	0	[-30,30]	30
Tip Blending Strength	1	[0.5, 1.5]	0.62

One possible formulation of a generic approximation model is as follows:

$$\hat{f} = \mathbf{w}^T \mathbf{\psi} \tag{2}$$

The vectors w and ψ denote weight and basis functions, respectively. if the orthogonal basis functions are selected as follows:

$$\psi^{i} = \exp(-\sum_{i=1}^{k} \theta_{j} |x_{j}^{i} - x_{j}|^{p_{j}})$$
(3)

The estimated function is the Kriging model. The basis function in Equation 3 indicates the correlation of random variables with $Y(x^i)$ evaluations in a sample set x^i . The basis function is mathematically stated as:

$$cor[Y(x^{i}), Y(x^{k})] = \exp(-\sum_{i=1}^{k} \theta_{j} |x_{j}^{i} - x_{j}^{k}|^{p_{j}})$$
 (4)

Covariance matrices can be expressed as:

$$Cov[\mathbf{Y}, \mathbf{Y}] = \sigma^2 \Psi$$
 (5)

Table 4 – Optimization Results

	L/D
Baseline	6
Optimized wingtip	6.76
Improvement	11%

Eventually, the wingtips design that have been improved regarding aerodynamics are presented. The CAD model and the geometrical specifications of the nonplanar tip-section optimized BWB model are provided in Table 5 and Figure 2.

Table 5 – Geometrical specifications

Parameter	Value
Aspect ratio, AR	3.879
LE inboard sweep angle, $\Lambda_{LEI}^{ o}$	58
LE outboard sweep angle, $\Lambda_{LEO}^{ o}$	40
Tapered wingtip sweep angles, $\Lambda_{LE,TE}$ o	56.4
TE sweep angle, Λ_{TE}	30
Airfoil profile	NACA 64 ₁ 212

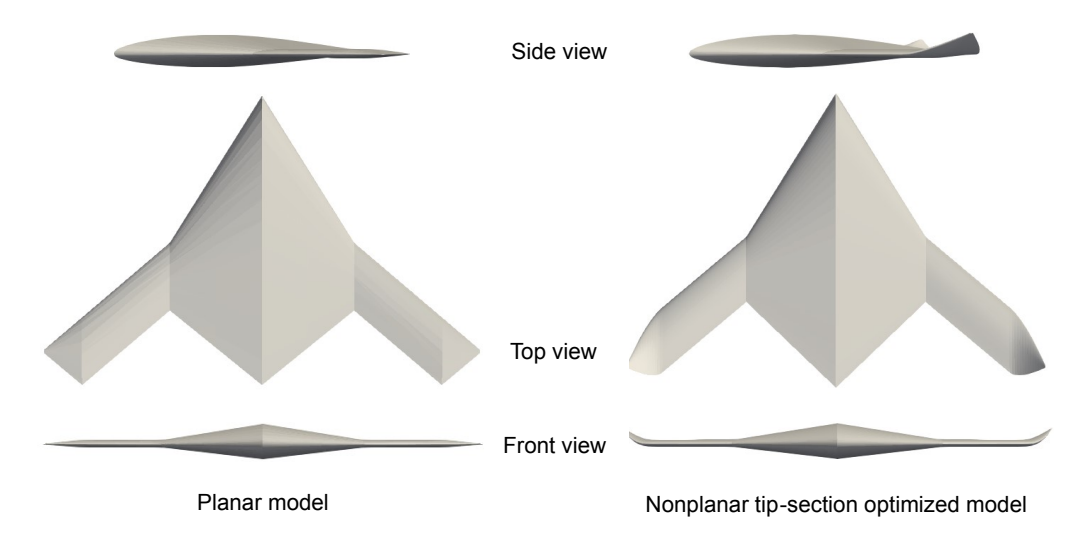


Figure 2 – Different views for planar BWB model (left) and nonplanar BWB Model (right)

The effect of the nonplanar wingtip section on the aerodynamic characteristics of the swept back flying BWB model was analyzed using the C_L/C_D ratio. The C_L/C_D comparison for the baseline planar tip-section and nonplanar tip-section optimized model is shown in (Figure 3). The nonplanar tip-section optimized model enhances the C_L/C_D by 11 and 7% at 0 and 5°, respectively, compared to the planar tip-section model. Moreover, the nonplanar tip-section optimized model shows an overall average improvement in C_L/C_D by 2.8%, compared to the planar tip-section model.

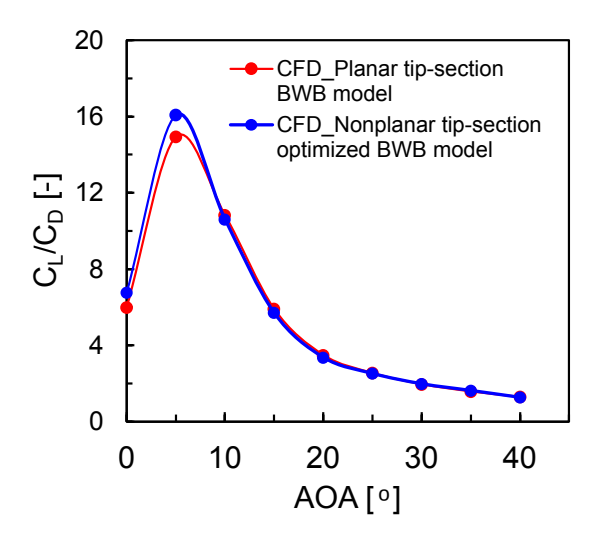


Figure 3 – Comparison of C_L/C_D curves of planar model and nonplanar tip-section models

3. Model Manufacturing and Wind Tunnel Testing

The aerodynamic performance of the optimized wingtip section design was tested in the wind tunnel at subsonic conditions. The rapid prototyping based on the fused deposition 3D printing technique with a white polylactide thermoplastic material was used to produce the model for testing (Figure 4). The model fabrication is elaborately discussed in [24] and not repeated here for brevity. Moreover, the present model has metallic inserts to improve the structural rigidity similar to the earlier fabricated wind tunnel model discussed in [24]. After the additive manufacturing process is completed, post-processing is carried out. Then, the wing model is assembled before being mounted on the sting system in the wind tunnel test section. The geometrical specifications of a 1:20 scaled-down nonplanar swept back flying BWB model are provided in Table 6.

Table 6 – Geometrical specifications.

Parameter	Value
Wing Area, $S m^2$	0.145
Wing Span, b m	0.75
Aspect ratio, AR	3.879
LE inboard sweep angle, Λ_{LEI} o	58
LE outboard sweep angle, Λ_{LEO} o	40
Tapered wingtip sweep angles, $\Lambda_{LE,TE}$ o	55, 30
TE sweep angle, Λ_{TE}	40
Airfoil profile	NACA 64 ₁ 212

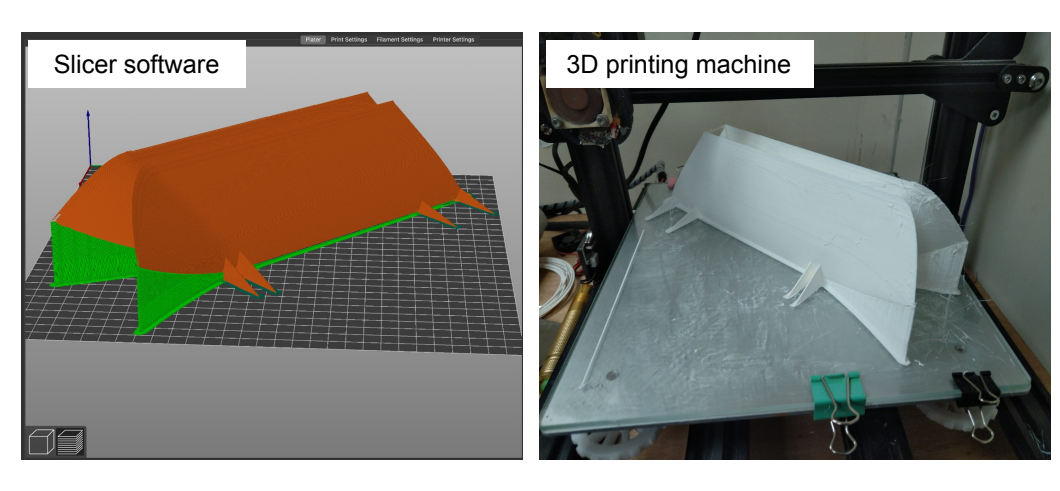


Figure 4 – PrusaSlicer [25] (left) and 3D printing (right).

This experimental study aimed to predict the aerodynamic performance of swept back flying BWB models. The aerodynamic forces and moments measurements on the models were performed in the de Havilland low-speed subsonic wind tunnel at the University of Glasgow [26]. The detailed specifications of the de Havilland wind tunnel test and conditions are presented in Tables 7 and 8, respectively. The installation of the present models in the wind tunnel for testing is shown in Figure 5. Airspeed and AOA were manually entered during testing. Afterward, the models in the tunnel, airspeed, and AOA were observed while the data was gathered from LabView program windows.

Table 7 – de Havilland wind tunnel specifications.

Location	Glasgow
Type of tunnel	a closed -return atmospheric low-speed
Test section	2.65 m × 2.1 m × 5.4 m
Test section shape	Octagonal cross-section
Maximum air speed	70 m/s
Maximum Mach number	0.2
Maximum Reynolds number	4×10^6
Contraction ratio	5:1
The inlet turbulence intensity	< 1%
Total pressure	1 bar
Pressure	Up to 2.94 kN/m ²
Temperature	Ambient to 300K
Equipment	6-component balance, sting and positioning system,
	and data acquisition system
Model support	Platform load cell beneath working section, and various
	capacity load cells
Outputs for the present test	Forces and moments

Table 8 – Wind tunnel test conditions.

Flow range $0-40^{\circ}$ AOA with step of 5° Test speed 30 m/s

Average air temperature 20°C

Average atmospheric pressure $1.125 \times 10^6 kN/m^2$





Figure 5 – Installation of planar and nonplanar BWB models in the wind tunnel test section

4. Computational Methodology

The flow domain was created similarly to the wind tunnel test section to investigate the aerodynamic performance of swept back flying BWB models (Figure 6). Table 9 provides the various steps involved in the CFD modelling used in the present work. Table 10 provides the specifications of the present numerical study, including the applied boundary conditions. Readers are suggested to refer to the authors' earlier works [22, 23, 24, 27, 28, 29] for a detailed explanation of CFD modeling.

Table 9 – Computational work stages.

Geometry modeling	 3D CAD models generated with SolidWorks [30] and exported as STEP files. Pre-processing done in Salome [31] to split and group the surfaces, and then exported in STL format for meshing.
Grid generation [32]	 Hexahedral background mesh produced from blockMesh. snappyHexMesh used to create flow domain mesh from background mesh and STL files.
Flow simulation [32]	 The simpleFOAM solver available in Open-FOAM 8.0 is used for simulations.
CFD validation	The CFD results were validated against the experimental test data.

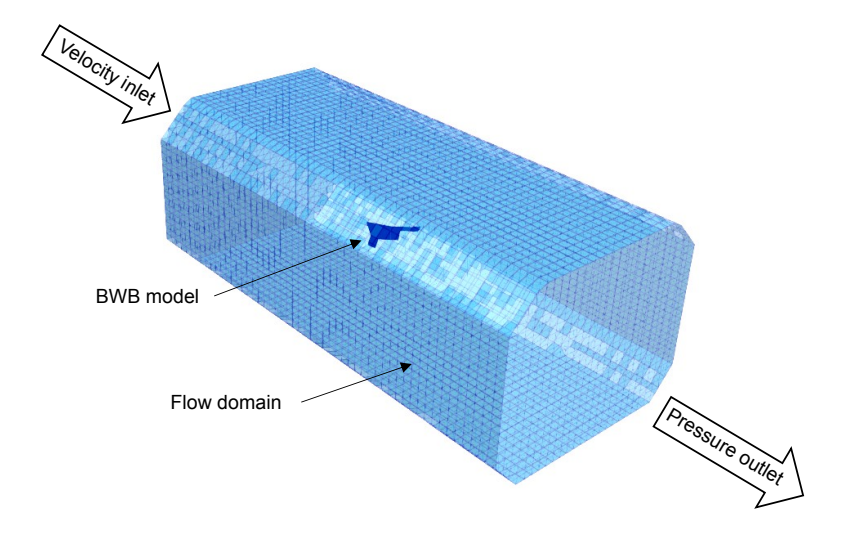


Figure 6 – 3D view of meshed domain

Table 10 – Specifications of numerical study.

Working fluid	Air
Type of analysis	Steady state
Nature of flow	Incompressible
Computational domain	Full span model
Turbulence model	k - ω SST model
Inlet turbulence intensity	0.5%
Intlet	Velocity inlet (30 m/s)
Outlet	Pressure outlet
Wing model	No-slip wall
Top, bottom, and side faces	Slip wall
Residual convergence	10^{-6}
Under-relaxation factors	Pressure (p) and Omega (ω) = 0.3 Velocity (U) and Turbulent kinetic energy (k) = 0.7

5. Results and discussion

5.1 Aerodynamic Coefficients

Figure 7 shows the aerodynamic characteristics comparison between the planar and nonplanar swept back flying BWB models, such as the lift coefficients (C_L) , drag (C_D) , pitching moment (C_{PM}) , yawing moment (C_{YM}) and rolling moment (C_{RM}) . The C_L curves shown in Figure 7a demonstrate similar lift values for both cases when the AOA $\leq 10^{\circ}$. For AOA $> 10^{\circ}$, the nonplanar tip-section model exhibits enhanced lift due to the reduction in induced drag, and a maximum increment of 4.2% is obtained at 25° AOA. For both models, the overall lift nonlinearly increases as AOA increases, and a stall occurs at a critical AOA (=35°). Figure 7b shows the C_D curves comparison, which reveals a similar trend for both models. The C_D increases with an increase in AOA and rapidly increases for AOA $\geq 10^o$ due to the increased flow separation. Notably, the nonplanar tip-section model shows significant drag reduction (\approx 8.5%) for 0 and 5° AOA. Figure 7c compares C_L against C_D for planar and nonplanar models. The figure shows no significant difference between the lift values for a C_D value ≤ 0.2 for both models. In contrast, the nonplanar tip-section model exhibits enhanced lift for the same drag value. The variation of C_{PM} with AOA for both configurations is illustrated in Figure 7d. As shown in the figure, the C_{PM} curve of the planar wing model exhibits a nonlinear trend with the onset of pitch-up (nose-up moment) at 5° AOA due to the tip stall, and it increases with AOA up to 15° AOA. Beyond 15° AOA, the pitching moment reduces as AOA increases. In contrast, the nonplanar configuration demonstrates smoother pitching moment characteristics without pitch-up or pitch-break compared to

the planar model. Figure 7e shows the behavior of C_{YM} against various AOA for planar and nonplanar configurations. The C_{YM} plots for both configurations show similar and insignificant yawing moments for AOA 0 and 15°. However, the planar configuration shows an increase in the C_{YM} values between 15 and 20° AOA. Beyond 20° AOA, there is no notable change in the C_{YM} with AOA. On the other hand, the nonplanar tip-section model C_{YM} fluctuates mildly at AOA $\geq 15^{\circ}$. Lastly, the behavior of C_{RM} plots against various AOA for both configurations is shown in Figure 7f. For the planar configuration, the C_{YM} is flat for the AOA 0-10° and $\geq 25^{\circ}$. However, the plot oscillates mildly with the AOA between 10 and 25° AOA. Conversely, the nonplanar wing model demonstrates no change in the C_{YM} curve at AOA $\leq 15^{\circ}$. The C_{YM} plot exhibits an oscillatory behavior between 15 and 25° AOA and it decreases with AOA increase at further than 25° AOA.

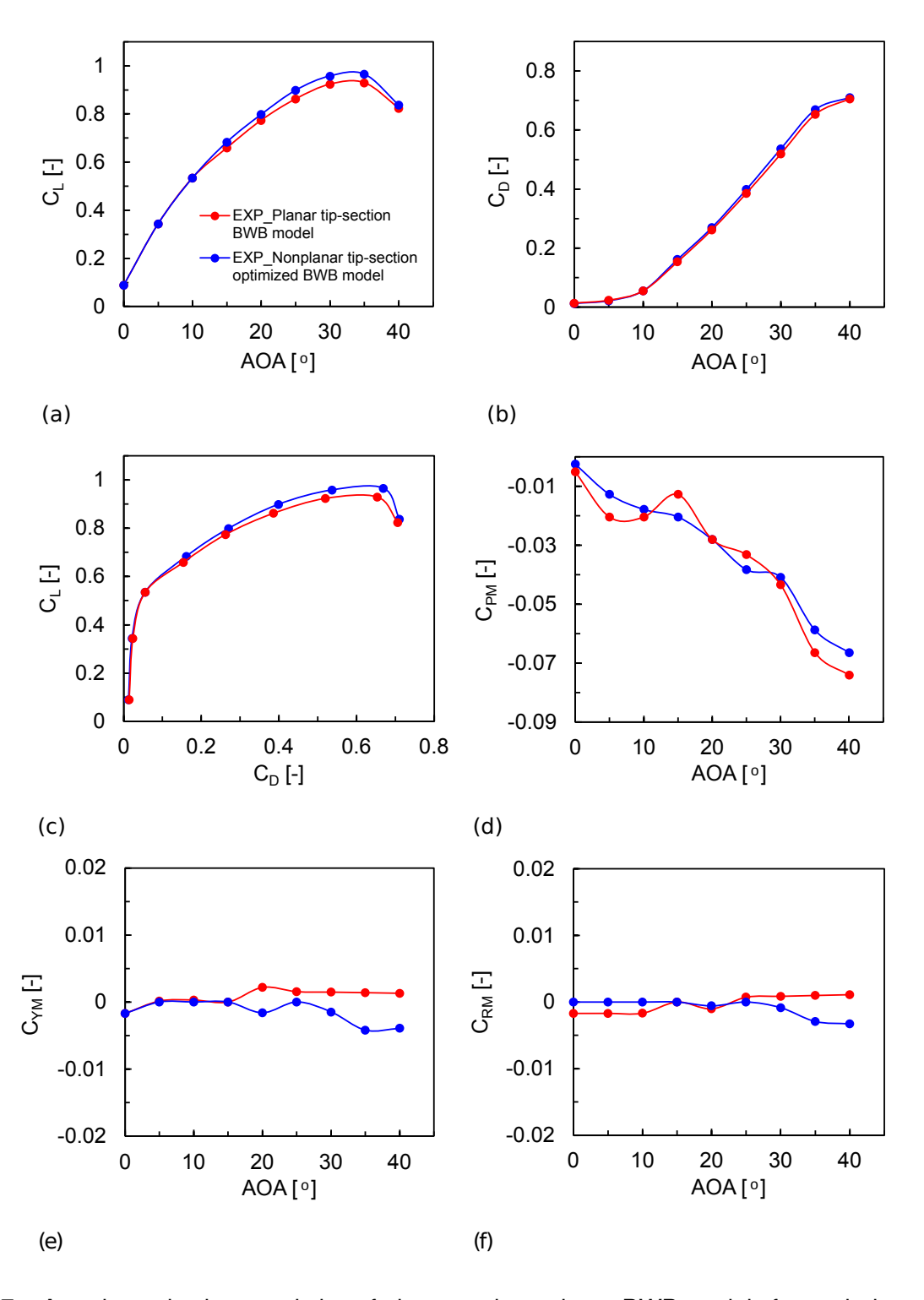


Figure 7 – Aerodynamic characteristics of planar and nonplanar BWB models from wind tunnel test.

5.2 Validation

The aerodynamic performance of the tip-section optimized model obtained from the CFD analysis is compared against the experimental data to ensure the accuracy of the CFD prediction. Figure 8 provides the C_L and C_D versus AOA plots for both experiment and CFD approach. As shown in figure, the trend and value of the lift (Figure 8)a and drag (Figure 8)b show satisfactory agreement with the experimental values. The CFD simulation accurately predicted the stall point value (=35°) which is crucial for the present investigation. Moreover, it can be concluded that the present CFD model is accurate enough to investigate the aerodynamic performance of the optimized tip section model.

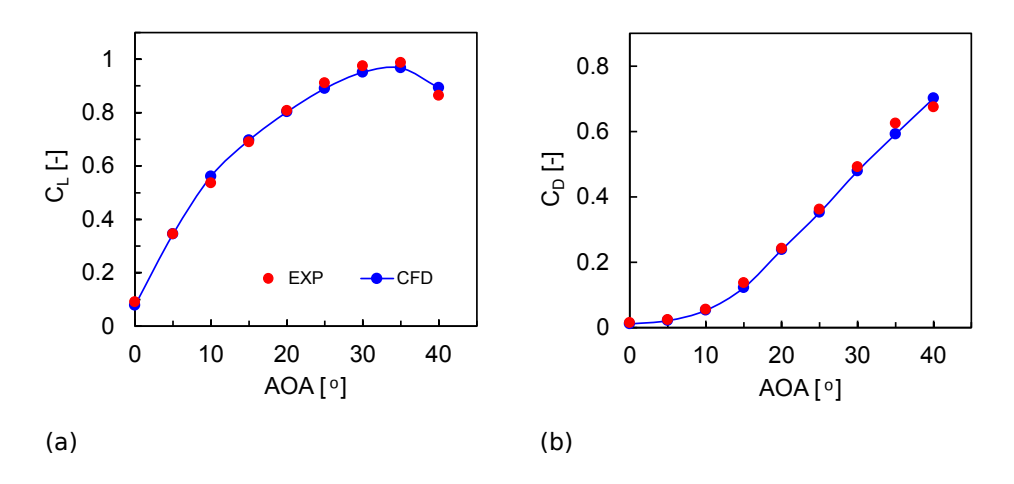


Figure 8 – Validation of CFD with Experimental data for the nonplanar tip-section optimized model.

5.3 Flowfield Comparison: Baseline vs Optimized Design

Figure 9 displays the Cp distribution with wall shear streamlines for various AOA values. At AOA = 10° , the nonplanar tip-section optimized model exhibits reduced suction near the tip region owing to the non-planarity of the tip-section. The reduced suction aids in suppressing the tip vortex strength. For AOA= 15° , we can see an expanded vortex for the nonplanar tip-section optimized model compared to the baseline case, indicating reduced vortex strength. As AOA increases (= 20°), the nonplanar tip-section optimized wing model shows reduced pressure suction in the inboard and outboard vortex interaction compared to the baseline planar model.

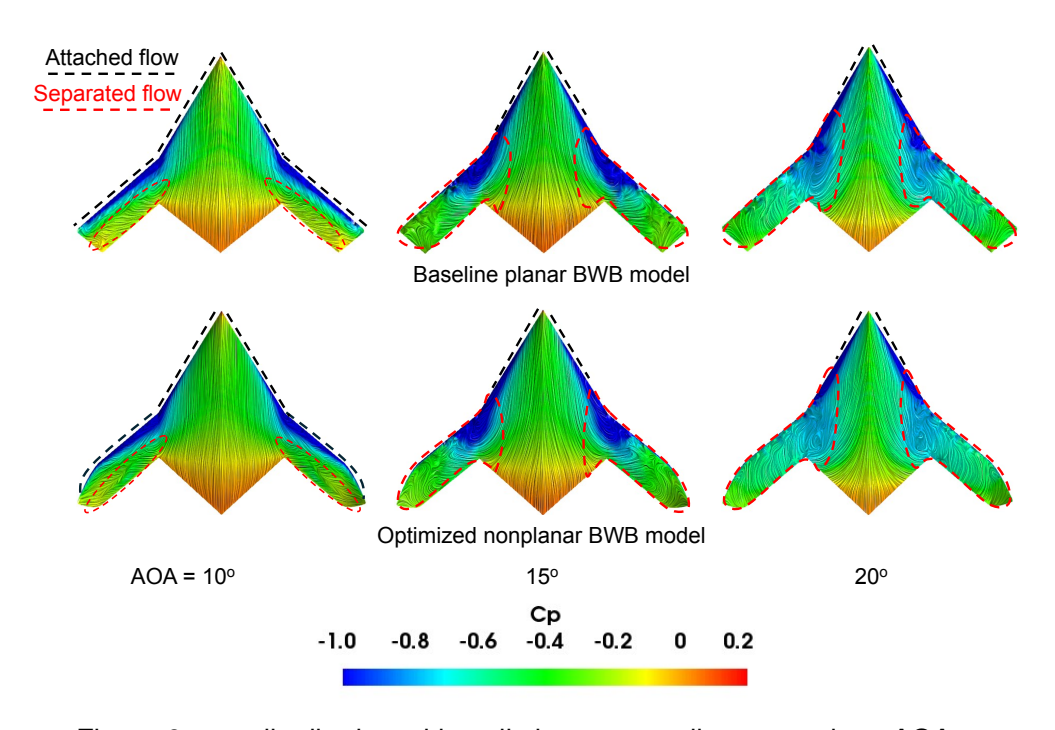


Figure 9 – C_p distribution with wall shear streamlines at various AOA.

To further understand the vortical flow structures, the suction surface vortex structures are visualized using the Q criterion (=35000 s⁻²) (Figures 10). As evident in the figure, the tip vortex is suppressed in the optimized model at AOA = 10° . As the AOA increases, the optimized model shows reduced vortex interaction between the inboard and outboard vortex which results in delayed stall and improved lift.

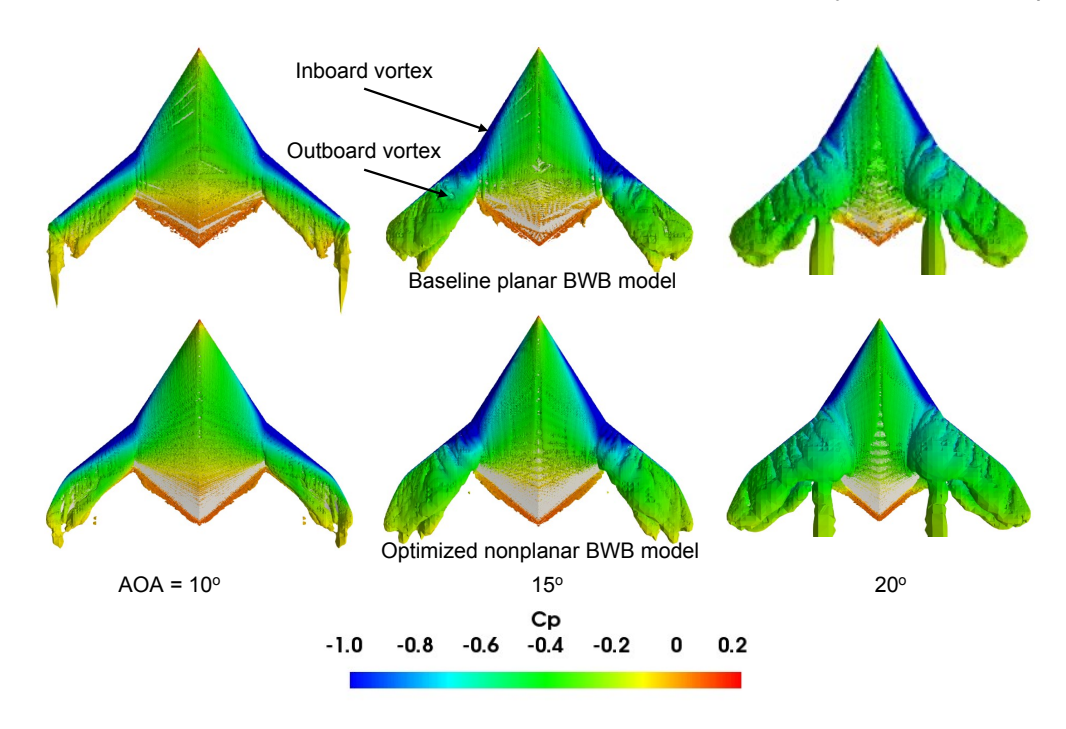


Figure 10 – The iso-surface of Q criterion (=35000 s^{-2}) coloured by C_p distribution at various AOA.

6. Conclusion

A mixture of low-speed wind tunnel testing and computational investigations were carried out to study the aerodynamic characteristics of planar and nonplanar swept back flying BWB models at different angles of attack. The advantage of high lift-to-drag ratio aerodynamic features in the swept back flying blended wing body type is due to their leading-edge vortex's aerodynamic features. The movement of the vortex causes the nonlinear behavior of the pitching moments. The nonplanar tip-section wing model exhibited an enhanced aerodynamic lift-to-drag ratio compared to the planar tip-section wing model. The planar tip-section wing model experienced the onset pitch-up at 5^o due to tip stall. In contrast, the nonplanar tip-section optimized wing model exhibited an improved pitching moment. Compared to the baseline planar model, the nonplanar tip-section optimized wing model shows reduced pressure suction in the inboard and outboard vortex interaction which leads to delayed stall and enhanced lift. Additionally, the present study serves as a foundation for additional optimization investigations, followed by computational and experimental investigations to develop the nonplanar mid-section flying BWB concept.

7. Acknowledgments

The authors would like to acknowledge NATO STO Support Project AVT-SP-002 Turbulence and the Aerodynamic Optimization of Nonplanar Lifting Systems.

8. Contact Author Email Address

The contact author email address is hsn.aleisa@gmail.com

9. Copyright Statement

The authors confirm that they, and/or their company or organization, hold copyright on all of the original material included in this paper. The authors also confirm that they have obtained permission, from the copyright holder of any third party material included in this paper, to publish it as part of their paper. The authors confirm that they give permission, or have obtained permission from the copyright

holder of this paper, for the publication and distribution of this paper as part of the ICAS proceedings or as individual off-prints from the proceedings.

References

- [1] Kuntawala N, Hicken J, and Zingg D. Preliminary aerodynamic shape optimization of a blended-wing-body aircraft configuration. 49th AIAA Aerospace Sciences Meeting including the New Horizons Forum and Aerospace Exposition, Orlando, Florida, 2011-642, pp 1-15, 04 January 2011 07 January 2011. https://doi.org/10.2514/6.2011-642
- [2] Lyu Z and Martins J R. Aerodynamic design optimization studies of a blended-wing-body aircraft. *Journal of Aircraft*, Vol. 51, No. 5, pp 1604-1617, September 2014. https://doi.org/10.2514/1.C032491
- [3] Kroo I. Nonplanar wing concepts for increased aircraft efficiency. *Innovative configurations and advanced concepts for future civil aircraft*, VKI Lecture Series, von Karman Inst., Rhode-Saint-Genèse, Belgium, June 6–10 2005.
- [4] Whitcomb R T. A design approach and selected wind tunnel results at high subsonic speeds for wing-tip mounted winglets. NASA-TN-D-8260, 1976. https://ntrs.nasa.gov/citations/19760019075
- [5] Heyson H, Riebe G, and Fulton C. Theoretical parametric study of the relative advantages of winglets and wing-tip extensions. NASA-TP-1020, 1977. https://ntrs.nasa.gov/citations/19770026168
- [6] Jones R, and Lasinski T. Effect of winglets on the induced drag of ideal wing shapes. Hampton: NASA, 1980.
- [7] Smith L A. Effects of winglets on the drag of a low-aspect-ratio configuration. Vol. 3563, NASA, Langley Research Center, 1996.
- [8] Spillman J. The use of wing tip sails to reduce vortex drag. *The Aeronautical Journal*, Vol. 82, No. 813, pp 387-395, 1978. https://doi.org/10.1017/S0001924000091168
- [9] Spillman J, Ratcliffe H, and McVitie A. Flight experiments to evaluate the effect of wing-tip sails on fuel consumption and handling characteristics. *The Aeronautical Journal*, Vol. 83, No. 823, pp 279–281, 1979. https://doi.org/10.1017/S0001924000031778
- [10] Spillman J, and McVitie A. Wing tip sails which give lower drag at all normal flight speeds. *The Aeronautical Journal*, Vol. 88, No. 878, pp 362–369, 1984. https://doi.org/10.1017/S000192400002087X
- [11] Spillman J. Wing tip sails; progress to date and future developments. *The Aeronautical Journal*, Vol. 91, No. 910, pp 445–453, 1987. https://doi.org/10.1017/S0001924000050624
- [12] Hackett J. Vortex drag reduction by aftmounted diffusing vanes. 12th International Council of the Aeronautical Sciences, Munich, Germany, Vol. 12, pp. 542–53, 1980.
- [13] Kroo I. A general approach to multiple lifting surface design and analysis. Aircraft Design Systems and Operations Meeting, San Diego, CA, USA, Vol. 10, No. 2514/6.1984-2507, pp. 2507, 31 October-02 November 1984. https://doi.org/10.2514/6.1984-2507
- [14] Smith M, Komerath N, Ames R, Wong O, and Pearson J. Performance analysis of a wing with multiple winglets. 19th AIAA Applied Aerodynamics Conference, Anaheim,CA,USA, Vol. 10, No. 2514/6.2001-2407, pp. 2407, 11 June 2001 14 June 2001. https://doi.org/10.2514/6.2001-2407
- [15] Céron-Muñoz H D, Cosin R, Coimbra R F D F, Correa L G N, and Catalano F M. Experimental investigation of wing-tip devices on the reduction of induced drag. *Journal of Aircraft*, Vol. 50, No. 2, pp 441-449, 30 Mar 2013. https://doi.org/10.2514/1.C031862
- [16] Yahyaoui M. A Comparative aerodynamic study of nonplanar wings. *International Journal of Aviation, Aeronautics, and Aerospace*, Vol. 6, No. 4, pp 10, 2019. https://doi.org/10.15394/ijaaa.2019.1383
- [17] Merryisha S and Rajendran P. Review of winglets on tip vortex, drag and airfoil geometry. *Journal of Advanced Research in Fluid Mechanics and Thermal Sciences*, Vol. 63, No. 2, pp. 218–237, 2019.
- [18] Verstraeten J, and Slingerland R. Drag characteristics for optimally span-loaded planar, wingletted, and C wings. *Journal of aircraft*, Vol. 46, No. 3, pp 962-971, 2009. https://doi.org/10.2514/1.39426
- [19] Ceron-Muñoz H, Diaz-Izquierdo D, Solarte-Pineda J, and Catalano F. Aerodynamic interference of wingtip and wing devices on BWB model. *29*th *International congress of the aeronautical sciences*, st. Petersburg, Russia, 7-12 September 2014.
- [20] Cerón-Muñoz H and Santana L. Experimental analyses of droop, wingtips and fences on a BWB model. Proceedings of the 30th Congress of the International Council of the Aeronautical Sciences Daejeon, Korea, pp. 25–30, 2016.
- [21] Furlong G C and Mchugh J G. A summary and analysis of the low-speed longitudinal characteristics of swept wings at high Reynolds number. NACA-TR-1339, 1957. https://ntrs.nasa.gov/citations/19930091013

- [22] Aleisa H, Kontis K, Nikbay M, Berkay P, Enes C and Emre K. Conceptual configuration of non-constant sweep UCAV concept. AIAA AVIATION Forum, Chicago, IL and Virtual, 10.2514/6.2022-3374, pp 1-20, June 27-July 1, 2022.
- [23] Aleisa H, Kontis K, Berkay P, and Nikbay M. Conceptual design of a nonconstant swept flying wing unmanned combat aerial vehicle. *Journal of Aircraft*, Vol. 60, No. 6, pp 1-17, November–December 2023. https://doi.org/10.2514/1.C037257
- [24] Aleisa H, Kontis K, Nikbay M. Low observable uncrewed aerial vehicle wind tunnel model design, manufacturing, and aerodynamic characterization. *Aerospace* Vol. 11, No. 216, 2024. https://doi.org/10.3390/aerospace11030216
- [25] PrusaSlicer|Original Prusa 3D printers directly from Josef Prusa, 2023. https://doi.org/https://www.prusa3d.com/.
- [26] National Wind Tunnel Facility/deHavilland low speed wind Tunnel.https://www.nwtf.ac.uk/facility/dehavilland-low-speed-wind-tunnel/ (accessed on 13 May 2023).
- [27] Aleisa H, Kontis K and Nikbay M. Identification of aerodynamic characteristics of generic UCAV configurations for low-speed flows. 11th Ankara International Aerospace Conference, METU, Ankara Turkey, AIAC-2021-081, pp 1-14, 8-10 September 2021.
- [28] Aleisa H, Kontis K and Nikbay M. Predictions of the low-speed aerodynamic characteristics of generic UCAVs. *AIAA SciTech Forum*, San Diego, CA and Virtual, 10.2514/6.2022-0428, pp 1-13, January 3-7, 2022.
- [29] Aleisa H, Kontis K, and Nikbay M. Numerical investigations on low-speed aerodynamic characteristics of generic unmanned combat aerial vehicle configurations. *Journal of Aircraft*, Vol. 60, No. 6, pp 1-11, November–December 2023.
- [30] SolidWorks. https://www.solidworks.com/.
- [31] Salome 2019 preprocessing package. https://www.salome-platform.org/.
- [32] Greenshields C, OpenFOAM user guide Version 8, The OpenFOAM Foundation, Vol. 237, 2020. https://doi.org/https://www.openfoam.com/.